



## Direct template synthesis of mesoporous carbon and its application to supercapacitor electrodes

Songhun Yoon<sup>a,\*</sup>, Seung M. Oh<sup>b</sup>, Chulwee Lee<sup>a</sup>

<sup>a</sup>Advanced Chemical Technology Division, Korea Research Institute of Chemical Technology (KRICT), Sinseongno 19, Yuseong, Daejeon 305-600, Republic of Korea

<sup>b</sup>Research Center for Energy Conversion and Storage (RCECS), School of Chemical and Biological Engineering and Institute of Chemical Process, College of Engineering, Seoul National University, Seoul 151-744, Republic of Korea

### ARTICLE INFO

#### Article history:

Received 25 September 2008

Received in revised form 27 March 2009

Accepted 22 April 2009

Available online 9 May 2009

#### Keywords:

A. Amorphous materials

B. Chemical synthesis

D. Electrochemical properties

### ABSTRACT

A direct templating method which is facile, inexpensive and suitable for the large scale production of mesoporous carbon is reported herein. A meso-structure surfactant/silicate template was made in a solution phase and resorcinol–formaldehyde as a carbon precursor was incorporated into the template solution. After aging, carbonization and hydrofluoric acid (HF) etching, mesoporous carbon was obtained. Using X-ray diffraction, scanning and transmission electron microscopy and nitrogen sorption, the synthesis mechanism of the mesoporous carbon was elucidated. According to the small angle X-ray scattering measurements, the surface became smoother after the removal of the silica, indicating that the silica was mostly located at the pore surface of the carbon. Also, the calculation of the pore volume demonstrated that the silica was transferred into the pores of the carbon without structural collapse during HF etching. When the prepared mesoporous carbon was applied to a supercapacitor electrode, the rectangular shape of the cyclic voltammogram was less collapsed, even at a high scan rate, which is indicative of its high rate capability. This was due to the low resistance of the electrolyte in the pores ( $3.8 \Omega \text{ cm}^2$ ), which was smaller than that of conventional activated carbon electrodes and even comparable to that of ordered mesoporous carbon electrodes. This improved performance was probably due to the well developed mesoporosity and high pore connectivity of the prepared mesoporous carbon.

© 2009 Elsevier Ltd. All rights reserved.

### 1. Introduction

Various synthesis methods, such as catalytic activation, the carbonization of polymer blend/organic gels, the carbonization of polymer aerogels and the template method, have been developed in order to prepare mesoporous carbon materials [1]. Among them, the template method using porous solid silica templates has been widely investigated by many researchers. Ordered mesoporous silica (OMS) materials such as MCM-48, MCM-41, SBA-15, MCF and HMS have been utilized for the preparation of ordered mesoporous carbon (OMC) [2–10]. The outstanding properties of OMC have been observed in its application for gas separation, water purification, catalyst supports, adsorbents and the electrode materials of charge storage devices, such as supercapacitors, lithium ion batteries and fuel cells [2–5]. Although the characteristic mesoporosity and high pore connectivity of OMCs gave rise to the fast transport of electrolytes and adsorbents through their inter-connected mesopores, the preparation of OMS materials and the templating procedure using OMS remains complex and

delicate [10]. Furthermore, the OMS has usually been sacrificed during silica etching using hydrofluoric acid (HF) or NaOH, resulting in the high preparation cost of the OMC. Hence, it has become increasingly important to develop a simpler and easier direct templating method for the synthesis of mesoporous carbon. Along these lines, much effort has been made to develop effective direct templating methods [11–16]. Various carbon precursors, such as divinyl-benzene, phenylene, 1,4-bis (triethoxysilyl)benzene and block co-polymer surfactants themselves, have been employed in the direct templating method using a silica/surfactant template. Nevertheless, silica etching after carbonization to generate pores remains an inevitable process in all of these synthesis methods [11–13]. Recently, several examples of OMCs prepared using only an organic surfactant (soft template) have been reported [14–16]. In these methods, the interaction between the carbon precursor and surfactant originates from resol, which is a partially polymerized oligomeric state of resorcinol–formaldehyde (RF) brought about through hydrogen bonding. Using this interaction, OMC films were prepared after carbonization to remove the surfactant template.

In this work, the direct templating method is employed for the synthesis of mesoporous carbon, whose final form is a powder. Hence, the preparation method employed herein has the merit of

\* Corresponding author. Tel.: +82 42 860 7199; fax: +82 42 860 7389.

E-mail address: [yoonsun@kRICT.re.kr](mailto:yoonsun@kRICT.re.kr) (S. Yoon).

easy scale-up for industrial mass production. The meso-structure of the surfactant/silicate template is made in advance within the solution phase and the carbon precursor, RF, is incorporated on the outside of the micelle core. This ordered composite is polymerized, carbonized and etched to obtain mesoporous carbon. Using small angle X-ray diffraction (XRD), small angle X-ray scattering (SAXS), scanning electron microscopy (SEM), transmission electron microscopy (TEM) and the measurement of the pore size distribution, the pore formation mechanism in the mesoporous carbon is clarified. As an application of the prepared mesoporous carbons, the performance of supercapacitor electrodes is investigated.

## 2. Experimental

### 2.1. Preparation of materials

Fig. 1 shows a schematic description of the synthesis process. After dissolving cetyltrimethylammonium bromide (CTAB) and sodium hydroxide in deionized water, tetraethylorthosilicate (TEOS) as a silica source was added. The molar ratio of CTAB/TEOS/NaOH/H<sub>2</sub>O was 2/1/1/200. Under these highly alkaline (pH > 14) conditions, silicate exists in a multi-charged D4R (double four-ring, [Si<sub>8</sub>O<sub>20</sub>]<sup>8-</sup>) state and this anionic silicate interacts electrostatically with the cationic surfactant initially existing in a micelle and molecule state [8]. This solution was stirred at 40 °C for 2 h in order to generate a template that exists in the phase of the tubular meso-structure (H<sub>0</sub>) of CTAB/[Si<sub>8</sub>O<sub>20</sub>]<sup>8-</sup> as shown in Fig. 1 (CTAB/silicate) [8,9]. Another solution of resorcinol (R) and formaldehyde (F) was prepared with Na<sub>2</sub>CO<sub>3</sub> as a catalyst at a molar ratio of R/F/Na<sub>2</sub>CO<sub>3</sub>/H<sub>2</sub>O = 10/20/1/100. After this RF solution was allowed to react for several tens of minutes, the two solutions (the homogeneous template solution and the RF solution) were mixed at a molar ratio of R/TEOS = 1/1, stirred vigorously and aged at 85 °C for a week. During this period, the silicate transformed to silica *via* polymerization, while the RF sol was converted to a gel through a condensation reaction [17]. The resulting precipitate (CTAB/SiO<sub>2</sub>/RF) was filtrated, dried in air at 85 °C, and then carbonized at high temperature under an Ar atmosphere for 1 h to remove the CTAB and carbonize the RF gel. As a final step, the silica included in the carbonized composite was removed by HF. Final

carbon specimens carbonized at 600 (C-600), 800 (C-800) and 1000 °C (C-1000) were acquired. For comparison, a control carbon (C-1) was prepared without the CTAB/SiO<sub>2</sub> template and another control carbon (C-2) was prepared without CTAB.

### 2.2. Analysis of pores

The pore size distribution (PSD) was analyzed by N<sub>2</sub> adsorption measurements (Micromeritics ASAP 2010). The external morphology of the carbon was examined using SEM (JEOL JSM-840A), whereas the pore image was obtained by TEM (JEOL JEM-2010). SAXS and small angle XRD were performed at the 4C-1 line of the Pohang Accelerator Laboratory. The beam flux and size were 10<sup>12</sup> mm<sup>-2</sup> and 0.3 mm<sup>2</sup>, respectively. The data was corrected after the air and dark scattering.

### 2.3. Preparation of supercapacitor electrodes

To prepare the EDLC (electric-double-layer capacitor) electrode, a mixture of the prepared carbon, polytetrafluoroethylene (PTFE) binder, and Ketjenblack ECP-600JD (KB) (at a weight ratio of 10:1:1) was dispersed in iso-propyl alcohol and coated on a 1 cm × 1 cm stainless steel Exmet which was used as the current collector. It was shown that this amount of conducting materials (10 wt%) produced much higher electric conductivity than other ionic conductivity [2]. The resulting electrode plate was pressed and dried under vacuum at 120 °C for 12 h.

### 2.4. Evaluation of supercapacitor performance

The electrochemical performance of the composite carbon electrodes was analyzed with a three-electrode configuration in aqueous 2 M H<sub>2</sub>SO<sub>4</sub> electrolyte. A Pt flag and SCE (saturated calomel electrode) were used as the counter and reference electrodes, respectively. The inter-electrode gap between the working electrode and reference one was fixed at 0.5 cm. Cyclic voltammetry (CV) was conducted using an EG&G PARC 362 potentiostat in the potential range of 0.0–0.7 V (vs. SCE) with scan rates ranging from 5 to 50 mV s<sup>-1</sup>. The current in the cyclic voltammograms was divided by the scan rate to obtain the capacitance vs. potential profiles. To calculate the equivalent series

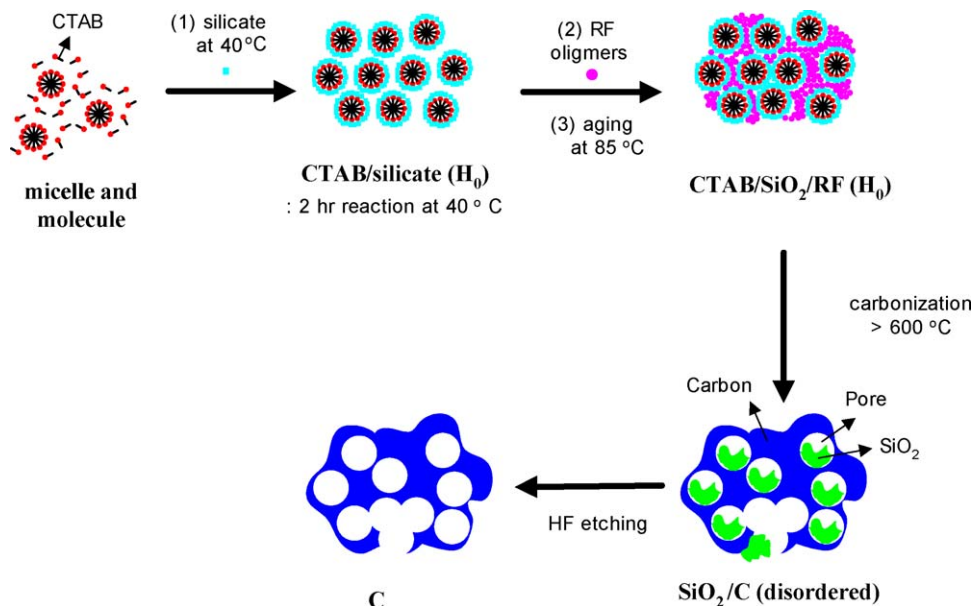


Fig. 1. Schematic explanation of synthesis. Notice that RF polymer was located at the outer part of CTAB/silicate micelles.

resistance (*ESR*) of the EDLC, a potential step of 10 mV was applied to the system after the stabilization of the potential at 0.2 V vs. SCE to 1  $\mu$ A.

### 3. Results and discussion

#### 3.1. Mechanism of direct templating

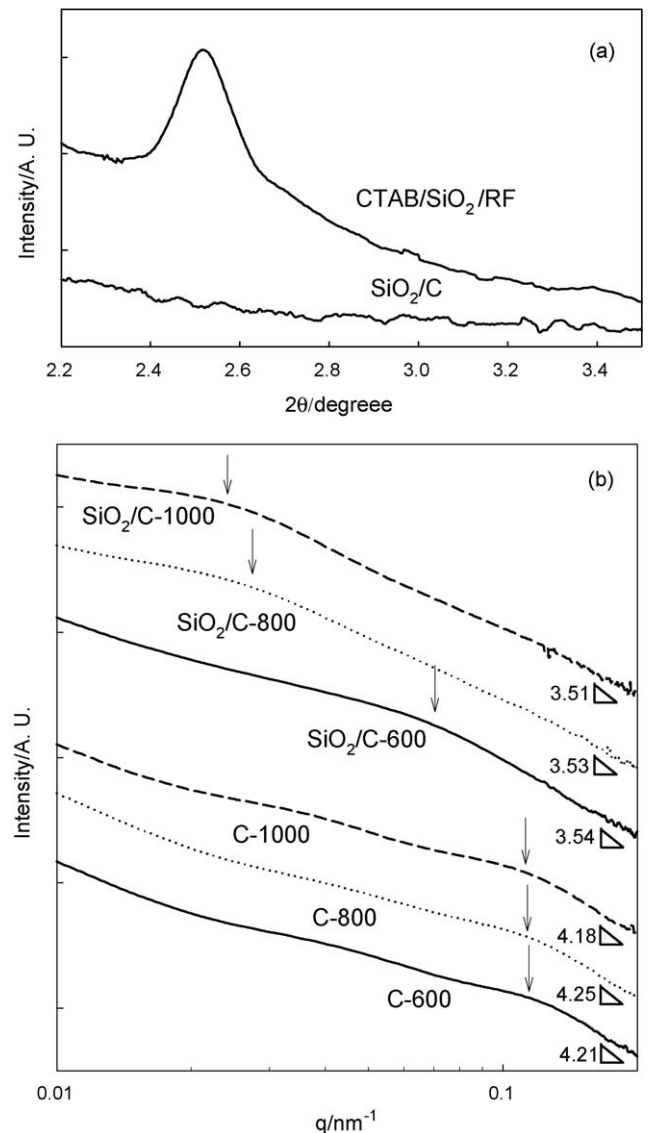
As shown in Fig. 1, under highly alkaline ( $\text{pH} > 14$ ) conditions, silicate exists in a multi-charged D4R (double four-ring,  $[\text{Si}_8\text{O}_{20}]^{8-}$ ) state and this anionic silicate interacts electrostatically with the cationic surfactant (CTAB) initially existing as rod-shaped micelles. It is well known that this interaction produces a hexagonal tubular structure ( $H_0$  phase), which is referred to herein as CTAB/silicate [9]. As reported by several researchers, a hexagonal tubular structure ( $H_0$ ) phase formed by the condensation between the rod micelles was observed at a reaction time of 5–6 min at 20 °C and a distinct hexagonal phase ( $H_1$ ) was observed after 20 h of reaction [17–23]. Similarly, it was observed from the cryo-TEM analysis that an ordered structure of SBA-15 was developed after 20 min [22]. From these literatures, therefore, it is concluded that the  $H_0$  phase is formed before a reaction time of 2 h under our preparation conditions. After the addition of the RF oligomers to the solution containing CTAB/silicate, CTAB/SiO<sub>2</sub>/RF was obtained after aging, filtration, washing and drying.

Fig. 2(a) shows the small angle XRD patterns of CTAB/SiO<sub>2</sub>/RF and SiO<sub>2</sub>/C. The latter (SiO<sub>2</sub>/C) was acquired from the carbonization of the former (CTAB/SiO<sub>2</sub>/RF) at 600 °C. The diffraction peak of CTAB/SiO<sub>2</sub>/RF was observed at 2.5°, which was similar to that of the CTAB/silicate phase, as shown in Fig. 1 ( $H_0$  phase) [8,9]. From the TEM analysis in Fig. 3(a), no isolated ordered phase associated solely with the silica/surfactant was observed, indicating that the RF oligomers were imbibed into the CTAB/silicate template at the molecular level. This result was similar to that of Zhao's group, where resol oligomers were incorporated into the hydrophilic portion of a block copolymer at the molecular level to produce OMC film [15]. In our experiment, an RF oligomer solution with a brownish color was formed after several tens of minutes. Also, it was observed that the gelation of the RF solution occurred when the reaction time exceeded 30 min, which is indicative of network formation between the RF oligomeric particles. Before gelation, the RF oligomers were added to the solution, in order to prepare a homogeneous composite material. It is well known that the particle size of the RF oligomer is very small, because of its high pH condition [32]. Since our RF oligomers had a similar structure to that of the resol oligomers, it was reasonable to assume that the RF oligomers were incorporated within the CTAB/silicate phase at the molecular level. After the carbonization of CTAB/SiO<sub>2</sub>/RF at temperatures ranging from 600 to 1000 °C, the silica/carbon composite (SiO<sub>2</sub>/C) was obtained. No diffraction peak for SiO<sub>2</sub>/C was observed, which is indicative of the collapse of the ordered structure. This disappearance of the ordered structure was probably due to the high thermal stress resulting from the large volume contraction (about 50%) during the carbonization of the RF polymer [24].

Although the ordered structure collapsed during the carbonization process, our templating method is easier and simpler when compared with the template method using solid porous silica. Also, since the mesoporous carbon was prepared inside a glass bottle on the bulk scale of several hundred grams, our preparation process of mesoporous carbon is suitable for scale-up.

#### 3.2. Small angle X-ray scattering (SAXS)

To investigate the change in the pore structure with the carbonization temperature, CTAB/SiO<sub>2</sub>/RF was carbonized at



**Fig. 2.** (a) Small angle X-ray diffraction patterns before carbonization (CTAB/SiO<sub>2</sub>/RF) and after carbonization (SiO<sub>2</sub>/C) at 600 °C. (b) Small angle X-ray scattering data of before (SiO<sub>2</sub>/C) and after HF etching (C). The carbonization temperature was 600 °C (solid line), 800 °C (dotted line) and 1000 °C (dashed line). The arrows represent crossover positions ( $q_c$ ).

temperatures ranging from 600 to 1000 °C and then the silica was removed by HF etching to acquire porous carbon materials (C). Fig. 2(b) presents the SAXS data of SiO<sub>2</sub>/C and C prepared at three different carbonization temperatures (600, 800 and 1000 °C). Note that the carbonization temperatures were included in the figure. From the SAXS experiment, it was found that the relationship between the measured intensity ( $I$ ) and scattering vector ( $q$ ) follows a power law;  $I(q) \propto q^{-(6-D)} = q^{-2}$  [25–27]. As  $q$  increases,  $z$  varies from the scattering of the mass fractal ( $z = 2$  from  $I \propto q^{-2}$ ) to the scattering of the surface fractal (Porod regime;  $z = 4$  from  $I \propto q^{-4}$ ) [26]. According to Bale and Schmidt, the fractal dimension indicating the surface roughness can be represented by  $n = N_0 r^{-D}$ . Here,  $D$ ,  $N_0$ ,  $r$  and  $n$  are the fractal (Hausdorff) dimension, the characteristic constant of the fractal surface, the length of the surface edge and the number of cubes comprising the surface, respectively [25]. Theoretically,  $D$  should be 2 for a perfectly smooth surface, while the larger the deviation from 2, the rougher the surface;  $z$  should have a value of 4 for perfectly smooth

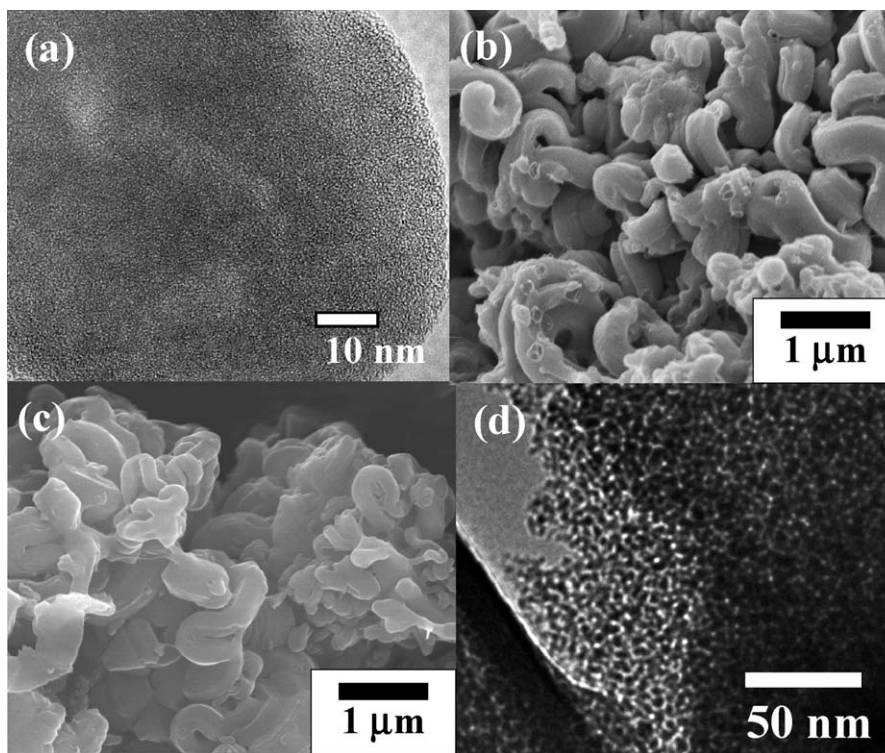


**Fig. 3.** TEM image: CTAB/SiO<sub>2</sub>/RF (a). FE-SEM images: SiO<sub>2</sub>/C (b) and C-1000 (c). TEM image: C-1000 (d). SiO<sub>2</sub>/C was obtained by carbonizing CTAB/SiO<sub>2</sub>/RF at 1000 °C.

surfaces, but  $z < 4$  for rough ones [26]. Hence, the pore surface roughness can be estimated from the measured value of  $z$  ( $z_s$ ) in the surface scattering regime (Porod regime:  $0.1 < q < 0.25$ ) [27]. Also, the size of the particles near the pore surface can be compared qualitatively from the crossover  $q$  value ( $q_c$ ), at which the change from scattering by the particles (mass scattering) to that by the particle surface (surface scattering in Porod regime) occurs [25].

In Fig. 2(b), the relationships of  $I(q)$  vs.  $q$  are plotted with sintering temperature and HF etching. In Table 1, the measured values of  $z_s$  and  $q_c$  are listed. Here,  $z_s$  increases from 3.5 for SiO<sub>2</sub>/C to 4.2 for C, irrespective of the carbonization temperature, indicating that the surface becomes smoother after the removal of the silica. This distinctive change of the surface roughness corresponds to the fact that the silica (SiO<sub>2</sub>) in SiO<sub>2</sub>/C is mostly located at the pore surface and is removed by HF etching (as shown in Fig. 1) to generate pores. The change of the crossover position ( $q_c$ ) in Table 1 indicates that the  $q_c$  of SiO<sub>2</sub>/C decreased with increasing carbonization temperature. Because of the increase in the sintering with increasing temperature, the SiO<sub>2</sub> located at the pore surface in SiO<sub>2</sub>/C was sintered to form larger particles (smaller  $q_c$ ). Furthermore, the  $q_c$  of porous carbon (C) was larger than that of SiO<sub>2</sub>/C and remained invariant, irrespective of the carbonization

temperature, which is indicative of a smaller particle size and negligible sintering (less particle growth).

### 3.3. Analysis of pore size distribution

Fig. 3(a) and (b) presents the morphologies of SiO<sub>2</sub>/C and C, respectively. Interestingly, similar tubular-shaped particles were observed in both SiO<sub>2</sub>/C and C [28]. In Fig. 3(d), the TEM image of carbon(C) indicated that it had a highly mesoporous structure, where the bright part corresponds to the mesopores. The observed pore shape was a wormhole-like one, which was assumed to be due to the collapse of the ordered structure after carbonization [29,30]. From the tubular particle shape and highly mesoporous structure of the resulting carbon (C), it was concluded that the CTAB/silicate played the role of a template to determine the particle shape of the resulting carbon and concomitantly to generate the pores in the carbon, as explained in Fig. 1.

In Fig. 4, the variations in the pore size distributions (PSD) of SiO<sub>2</sub>/C (empty circles) and C (filled circles) with the carbonization temperature (600, 800 and 1000 °C) are presented. The Barrett–Joyner–Halenda (BJH) method based on the adsorption branch was utilized to obtain the pore size distribution. Also, the surface area and pore volume of SiO<sub>2</sub>/C and C are listed in Tables 1 and 2, respectively. Apparently, the pore volume and surface area were increased significantly by removing the silica of SiO<sub>2</sub>/C for all carbonization temperatures. For comparison, a control carbon (C-1) was prepared without CTAB/SiO<sub>2</sub> and it showed nonporous properties (surface area;  $10 \text{ m}^2 \text{ g}^{-1}$ ), because the pore structure completely collapsed after carbonization (carbon xerogel). This nonporous property was attributed to the very small primary particle size of the RF polymer and lack of cross-linking induced by H<sup>+</sup> ions under high pH conditions [17,31,32] shown in Fig. 4 is the bimodal pore distribution of carbon. Although the reason for it is not clear, this bimodal distribution may originate from the

**Table 1**

The small angle X-ray scattering data and surface area of SiO<sub>2</sub>/C and C according to the carbonization temperature.

	SiO <sub>2</sub> /C			C		
	600	800	1000	600	800	1000
Carbonization temperature/°C	600	800	1000	600	800	1000
Slope in Porod regime, $z_s$	3.54	3.53	3.51	4.21	4.25	4.18
Crossover position, $q_c$	0.06	0.025	0.02	0.12	0.12	0.12
BET surface area, $S_{\text{BET}}/\text{m}^2 \text{ g}^{-1}$	131	108	100	756	598	568

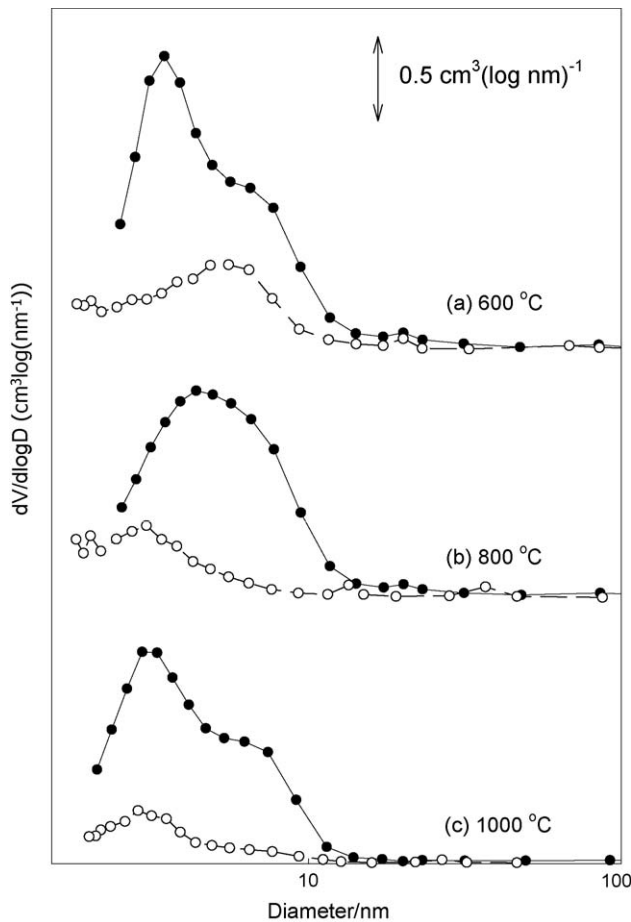


**Fig. 4.** The pore size distributions calculated by BJH method in  $N_2$  adsorption profiles. The carbonization temperature was (a) 600 °C, (b) 800 °C and (c) 1000 °C. The empty circle and filled one are the data measured before and after HF etching, respectively.

characteristic agglomeration of the CTAB/silicate micelles or partial phase separation between CTAB/SiO<sub>2</sub> and RF.

From further experiments, it was found that the pore size increased with increasing reaction time of CTAB/silicate before the addition of RF (not shown here). In addition, the particle size of the mesoporous carbon became smaller with decreasing CTAB surfactant concentration. This control of the mesoporous carbon porosity by changing the preparation conditions in the direct templating method will be addressed in a future report.

**Table 2**

The comparison between the calculated specific pore volume and the measured one in C after HF etching of SiO<sub>2</sub>/C.

	Carbonization temperature/°C		
	600	800	1000
SiO <sub>2</sub> /C			
$V_{\text{pore-b}}^{\text{mea}}/\text{cm}^3 \text{g}^{-1\text{a}}$	0.18	0.11	0.10
$V_{\text{SiO}_2\text{-b}}^{\text{cal}}/\text{cm}^3 \text{g}^{-1\text{b}}$	0.22	0.22	0.22
C			
$V_{\text{pore-a}}^{\text{cal}}/\text{cm}^3 \text{g}^{-1\text{c}}$	0.77	0.63	0.62
$V_{\text{pore-a}}^{\text{mea}}/\text{cm}^3 \text{g}^{-1\text{d}}$	0.76	0.66	0.59

<sup>a</sup> Measured specific pore volume in SiO<sub>2</sub>/C (before HF etching) based on BJH method.

<sup>b</sup> Calculated specific volume of SiO<sub>2</sub> in SiO<sub>2</sub>/C (before HF etching).

<sup>c</sup> Calculated specific pore volume in C (after HF etching).

<sup>d</sup> Measured specific pore volume in C (after HF etching) based on BJH method.

### 3.4. Estimation of pore conversion during HF etching

To clarify the pore formation of C after the HF etching of SiO<sub>2</sub>/C, the pore generation from SiO<sub>2</sub>/C into C was analyzed quantitatively as follows:

$$V_{\text{pore-b}}^{\text{cal}} = \frac{V_{\text{pore-b}}^{\text{mea}} + V_{\text{SiO}_2\text{-b}}^{\text{cal}}}{x_C} = \frac{V_{\text{pore-b}}^{\text{mea}}}{x_C} + \frac{x_{\text{SiO}_2}}{x_C} \frac{1}{d_{\text{SiO}_2}} \quad (1)$$

Here  $V_{\text{SiO}_2\text{-b}}^{\text{cal}}$  is the calculated specific volume of SiO<sub>2</sub> in SiO<sub>2</sub>/C (before HF etching),  $V_{\text{pore-b}}^{\text{mea}}$  is the measured specific pore volume in SiO<sub>2</sub>/C (before HF etching),  $V_{\text{pore-a}}^{\text{cal}}$  is the calculated specific pore volume in C (after HF etching),  $x_{\text{SiO}_2}$  is the weight fraction of SiO<sub>2</sub> in SiO<sub>2</sub>/C,  $x_C$  is the weight fraction of carbon in SiO<sub>2</sub>/C and  $d_{\text{SiO}_2}$  is density of SiO<sub>2</sub> in SiO<sub>2</sub>/C (2.2 g/cm<sup>3</sup>) [27].

From the thermogravimetric analysis (TGA) under Ar and air, it was found that SiO<sub>2</sub>/C was composed of 52 wt% carbon and 48 wt% silica ( $x_{\text{SiO}_2} = 0.48$ ,  $x_C = 0.52$ ). Using Eq. (1),  $V_{\text{pore-a}}^{\text{cal}}$  was compared with  $V_{\text{pore-a}}^{\text{mea}}$ , and the results are presented in Table 2. Irrespective of the carbonization temperature,  $V_{\text{pore-a}}^{\text{cal}}$  were very similar to  $V_{\text{pore-a}}^{\text{mea}}$ , indicating that the silica was located within the inner space of SiO<sub>2</sub>/C and was transferred into the pores of C without structural collapse during HF etching, showing the validity of the proposed mechanism in Fig. 1.

### 3.5. Performance of supercapacitor electrodes

In order to investigate the EDLC performance, electrodes was fabricated using the prepared mesoporous carbons. Typically, an EDLC utilizes the charge accumulated in the electric-double layer of the porous carbon electrodes [33]. The superior properties of EDLCs compared to batteries lie in their high rate performance and good cyclability. In previous papers, it has been revealed that the pore structure, such as the size and connectivity, significantly influence the rate performance of EDLCs, which is related to the electrolyte transport through the pores of the carbon electrodes [2–4]. Especially, because of their mesopores and high connectivity, electrodes fabricated from OMCs prepared using OMS templates such as MCM-48 and HMS showed superior rate performance to those made of conventional microporous activated carbon. Herein, the EDLC electrode performance of the mesoporous carbon prepared at 1000 °C (C-1000) was investigated. For comparison, another control carbon (C-2) was prepared without CTAB and HF-etched to remove the silica (pore diameter: ~1 nm, measured  $S_{\text{BET}} = 292 \text{ m}^2 \text{g}^{-1}$ ), showing microporous properties. The EDLC performances of the electrodes using the two carbons were compared.

Fig. 5 shows the capacitance vs. voltage profiles and chronoamperograms for the two carbon electrodes. Here, the capacitance vs. voltage profiles were acquired by dividing the measured current by the scan rate (5 and 50 mV/s) in the cyclic voltammograms [2,3]. From these profiles, the estimated specific capacitances ( $C_{\text{sp}}$ ) of C-2 and C-1000 were 20 and 50 Fg<sup>-1</sup>, respectively, indicating that  $C_{\text{sp}}$  was proportional to  $S_{\text{BET}}$  [34]. In an ideal capacitor, the capacitance vs. voltage profile should have a rectangular shape, irrespective of the scan rate. The collapse of the rectangular shape with increasing scan rate is highly influenced by the time constant ( $\tau$ ) of the EDLC electrode, which has the following relation between  $C_{\text{sp}}$  and ESR (equivalent series resistance);  $\tau = \text{ESR} \times C_{\text{sp}}$ . Importantly, the rate performance of EDLC electrodes is inversely proportional to  $\tau$  [2,3,35,36]. As seen in Fig. 5(a) and (c), the rectangular shape of the C-1000 electrodes collapsed less severely than that of C-2. When considering the higher  $C_{\text{sp}}$  of the C-1000 electrodes, it is probable that the observed lesser collapse of the rectangular shape was due to the smaller ESR.

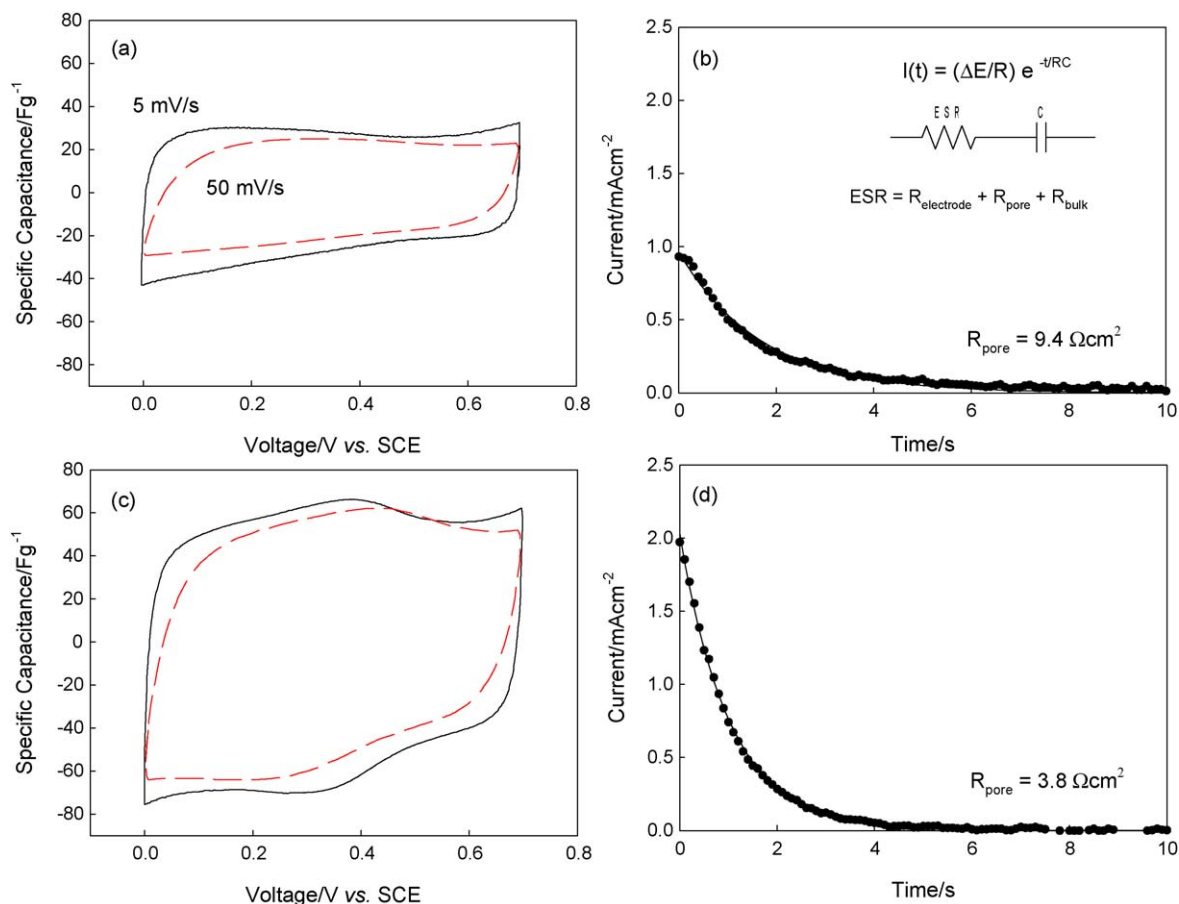


**Fig. 5.** (a and c) Capacitance vs. voltage profile obtained by cyclic voltammetry. (b and d) Typical current transient from a chronoamperometry experiment. Here,  $\Delta E$ ,  $R$  and  $C$  are potential step value, resistance ( $ESR$ ) and capacitance, respectively. (a and b) Mesoporous carbon prepared direct template methods (C-1000). (c and d) Control one (C-2).

### 3.6. Estimation of equivalent series resistance ( $ESR$ )

In order to estimate the  $ESR$ , chronoamperometry was conducted. For these measurements, a potential step (10 mV) was applied from 0.2 V and the subsequent current transient was recorded every 0.1 s (Fig. 5(b) and (d)) [2,3,37]. The base potential (0.2 V) that was used was selected because the effect of the pseudocapacitance arising from quinone–hydroquinone couples is negligible in this potential range [35]. The exponentially decaying current transients were fitted with the equation indicated in the inset of Fig. 5(b) and the  $ESR$  was obtained from this fitting. In the figure, the filled circles represent the sampled current, whereas the solid line corresponds to the best fitted one.

As expressed in the inset of Fig. 5(b), the  $ESR$  (equivalent series resistance) can be represented by  $ESR = R_{\text{electrode}} + R_{\text{pore}} + R_{\text{bulk}}$ . Here,  $R_{\text{electrode}}$ ,  $R_{\text{pore}}$  and  $R_{\text{bulk}}$  are the electronic resistance of the electrode, the electrolyte resistance in the pores and the bulk ionic resistance between the working and reference electrodes, respectively. After adding more than 7 wt% of carbon black as a conducting material,  $R_{\text{electrode}}$  was calculated to be as small as about  $0.02 \Omega \text{ cm}^2$ , which was negligible in the total  $ESR$  [2]. From the bulk electrolyte conductivity ( $0.68 \text{ S cm}^{-1}$ ) and inter-electrode gap between the working and reference electrodes (0.5 cm),  $R_{\text{bulk}}$  was calculated to be  $0.73 \Omega \text{ cm}^2$  [3]. Because the same cell structure was employed for both of them,  $R_{\text{electrode}}$  and  $R_{\text{bulk}}$  were invariant for the two carbon electrodes. After the extraction of  $R_{\text{bulk}}$  and  $R_{\text{electrode}}$  from the  $ESR$ ,  $R_{\text{pore}}$  was calculated. The estimated values of  $R_{\text{pore}}$  for C-1000 and C-2 were 3.8 and  $9.4 \Omega \text{ cm}^2$ , respectively. Hence, the lesser collapse of the rectangular shape in the capacitance vs. voltage profile was mostly attributable to the

low  $R_{\text{pore}}$  in the C-1000 electrodes. The low  $ESR$  of C-1000 was comparable to that of OMC electrodes using HMS or MCM-48 silica as a template ( $2.0$ – $2.9 \Omega \text{ cm}^2$ ), and is indicative of the presence of well developed mesopores and the high connectivity of the pores in our mesoporous carbon [2,3,30]. For the conventional activated carbon, MSC-25 (molecular sieving carbon), the measured  $ESR$  was  $4.92 \Omega \text{ cm}^2$  [2]. Hence, the high rate capability of our mesoporous carbon electrode was certainly attributable to its well developed mesoporosity and high pore connectivity, which survived even after the collapse of the ordered structure. Additionally, the direct templating method proposed herein is simpler and cheaper than the conventional template method using porous silica.

## 4. Conclusions

A silicate/surfactant template in the solution phase was utilized as a direct template for the preparation of mesoporous carbon. From the small angle XRD, SEM and TEM analyses, the synthesis mechanism of the mesoporous carbon was clarified. The structural change with the carbonization temperature was elucidated from the SAXS experiment. Because of its well developed mesoporosity, the prepared carbon exhibited improved rate capability, which was comparable to that of OMS electrodes.

## Acknowledgement

This research was supported by a grant from the Fundamental R & D Program for Core Technology of Materials funded by the Ministry of Knowledge Economy, Republic of Korea.

## References

- [1] T. Kyotani, *Carbon* 38 (2000) 269.
- [2] S. Yoon, J. Lee, T. Hyeon, S.M. Oh, *J. Electrochem. Soc.* 147 (2000) 2507.
- [3] J. Lee, S. Yoon, S.M. Oh, T. Hyeon, *Adv. Mater.* 12 (2000) 359.
- [4] J. Lee, S. Yoon, S.M. Oh, T. Hyeon, *Chem. Commun.* (1999) 2177.
- [5] S.H. Joo, S.J. Choi, I. Oh, J. Kwak, Z. Liu, O. Terasaki, *Nature* 412 (2001) 169.
- [6] C.T. Kresge, M.E. Leonowicz, W.J. Roth, J.C. Vartuli, J.S. Beck, *Nature* 359 (1992) 710.
- [7] D. Zhao, J. Feng, Q. Huo, N. Melosh, G.H. Fredrickson, G.H. Chmelka, G.D. Stucky, *Science* 279 (1998) 548.
- [8] J.Y. Ying, C.P. Mehnert, M.S. Wong, *Angew. Chem. Int. Ed.* 38 (1999) 56.
- [9] J. Xu, Z. Luan, H. He, W. Zhou, L. Kevan, *Chem. Mater.* 10 (1998) 3690.
- [10] J. Lee, J. Kim, T. Hyeon, *Adv. Mater.* 18 (2006) 2073.
- [11] I. Moriguchi, Y. Koga, R. Matsukura, Y. Teraoka, M. Kodama, *Chem. Commun.* (2002) 1844.
- [12] F. Zhang, D. Gu, Y. Yan, C. Yu, B. Tu, D. Zhao, *J. Am. Chem. Soc.* 127 (2005) 13508.
- [13] B.-H. Han, W. Zhou, A. Sayari, *J. Am. Chem. Soc.* 125 (2003) 3444.
- [14] S. Tanaka, N. Nishiyama, Y. Egashira, K. Ueyama, *Chem. Commun.* (2005) 2125.
- [15] Y. Meng, D. Gu, F. Zhang, Y. Shi, H. Yang, Z. Li, C. Yu, B. Tu, D. Zhao, *Angew. Chem. Int. Ed.* 44 (2005) 7053.
- [16] C. Liang, K. Hong, G.A. Guiocho, J.W. Mays, S. Dai, *Angew. Chem. Int. Ed.* 43 (2004) 5785.
- [17] R.W. Pekala, D.W. Schaefer, *Macromolecules* 26 (1993) 5487.
- [18] J. Zhang, D. Goldfarb, *Micropor. Mesopor. Mater.* 48 (2001) 143.
- [19] Q. Huo, D.I. Margolese, U. Ciesla, D.G. Demuth, P. Feng, T.E. Gier, P. Sieger, A. Firouzi, B.F. Chmelka, F. Schuth, G.D. Stucky, *Chem. Mater.* 6 (1994) 1176.
- [20] Y. Wan, H. Yang, D. Zhao, *Acc. Chem. Res.* 39 (2006) 423.
- [21] Y. Wan, Y. Shi, D. Zhao, *Chem. Commun.* (2007) 897.
- [22] Y. Wan, D. Zhao, *Chem. Rev.* 107 (2007) 2821.
- [23] R. Liu, Y. Shi, Y. Wan, Y. Meng, F. Zhang, D. Gu, Z. Chen, B. Tu, D. Zhao, *J. Am. Chem. Soc.* 128 (2009) 11652.
- [24] G. Savage, *Carbon–Carbon Composites*, Chapman & Hall, London, 1993, p. 121.
- [25] H.D. Bale, P.W. Schmidt, *Phys. Rev. Lett.* 53 (1984) 596.
- [26] V. Bock, A. Emmerling, J. Fricke, *J. Non-Cryst. Solids* 225 (1998) 69.
- [27] T.P. Reiker, S. Misono, F. Ehrburger-Dolle, *Langmuir* 15 (1999) 914.
- [28] A. Sayari, *J. Am. Chem. Soc.* 122 (2000) 6504.
- [29] C.C. Landry, S.H. Tolbert, K.W. Gallis, A. Monnier, G.D. Stucky, P. Nordy, J.C. Hanson, *Chem. Mater.* 13 (2001) 1600.
- [30] J. Lee, J. Kim, Y. Lee, S. Yoon, S.M. Oh, T. Hyeon, *Chem. Mater.* 16 (2004) 3323.
- [31] R.W. Pekala, *J. Mater. Sci.* 24 (1989) 3221.
- [32] C. Lin, J.A. Ritter, *Carbon* 35 (1997) 1271.
- [33] K. Kinoshita, *Carbon: Electrochemical and Physicochemical Properties*, John Wiley & Sons, New York, 1998, p. 12.
- [34] B.E. Conway, *Electrochemical Supercapacitors*, Kluwer Academic/Plenum Publisher, 1999, p. 125.
- [35] S. Yoon, J.H. Jang, B.H. Ka, S.M. Oh, *Electrochim. Acta* 50 (2005) 2255.
- [36] L. Li, H. Song, Z. Chen, *Electrochim. Acta* 51 (2006) 5715.
- [37] A.J. Bard, L.R. Faulkner, *Electrochemical Methods: Fundamentals and Applications*, John Wiley & Sons, New York, 1988, p. 15.